Colloids and Surfaces B: Biointerfaces 222 (2023) 113018

Contents lists available at ScienceDirect

Colloids and Surfaces B: Biointerfaces

journal homepage: www.elsevier.com/locate/colsurfb

Hydrogel forming microneedle-mediated transdermal delivery of sildenafil citrate from polyethylene glycol reservoir: An ex vivo proof of concept study

Diany Elim [a], Andi Maqhfirah Nurul Fitri [a], Muhammad Alif Sya'ban Mahfud [a], Nur Afika [a], Nurul Aisha Fitri Sultan [a], Hijrah [b], Rangga Meidianto Asri [a], Andi Dian Permana [a,*]

[a] Faculty of Pharmacy, Hasanuddin University, Makassar 90245, Indonesia
[b] Faculty of Medicine, Hasanuddin University, Makassar 90245, Indonesia

ARTICLE INFO

Keywords:
Erectile dysfunction
Hydrogel-forming microneedles
PEG reservoir
Sildenafil citrate

ABSTRACT

Erectile dysfunction (ED) is a disorder that often occurs in men worldwide. One of the drugs used as the first-line therapy for erectile dysfunction is sildenafil citrate (SC). Unfortunately, SC was commonly found in oral, injection, and transdermal dosage forms with some limitations, mainly related to low oral bioavailability caused by the occurrence of first-pass metabolism in the liver, and poor patient comfort and compliance. Therefore, it was essential to develop dosage forms to overcome these limitations. We developed hydrogel-forming microneedles (HFM) that can facilitate transdermal delivery of SC by penetrating the *stratum corneum*. HFM was made using polyvinyl alcohol (PVA) and polyvinyl pyrrolidone (PVP) as polymers and several variations of tartaric acid as crosslinking agents. The evaluation of swelling properties, mechanical resistance, and penetration ability showed that the HFM produced had good insertion properties and swelling capabilities ranging from 300% to 700%. This HFM was designed to be integrated with a polyethylene glycol (PEG) reservoir prepared using several types of PEG with different molecular weights. The *ex vivo* permeation study showed that up to 80% of SC (equivalent to 20.2 ± 0.29 mg/mL) was delivered transdermally from this combined dosage form. For the first time, SC has been successfully developed into an HFM that was integrated with a PEG reservoir which was non-irritating, safe, and painless. It also had promising results for increasing the effectiveness of ED therapy.

1. Introduction

Erectile dysfunction (ED) is a type of sexual disorder in men defined as the inability to achieve and maintain a sufficient erection for satisfactory sexual intercourse [1]. Usually associated with normal aging and illness, ED has affected up to 150 million men worldwide, with the prevalence and incidence being relatively higher in men over 40 years of age [2–4]. The prevalence of ED varies significantly in Asia, ranging from 2% to 81.8%. Specifically, the prevalence of ED in Indonesia has been reported to be 11% [5]. Even though ED has been generally considered not life-threatening, this condition was vital to treat because it significantly impacts the patient's quality of life, with one of the consequences being the loss of self-confidence and even depression [1]. In addition, ED can be a sign of other undiagnosed conditions, such as hypercholesterolemia and diabetes mellitus, and precede the manifestation of coronary artery disease within 3–5 years [6,7].

Among treatments available for ED, orally administrated phosphodiesterase-5 inhibitor (PDE5-I), such as sildenafil citrate (SC), has been a popular option due to their high efficacy, low cost in terms of patient convenience, as well as minimal side effect profile [6,8]. PDE5-I works by competitively inhibiting the PDE5 enzyme (responsible for the degradation of cyclic guanosine monophosphate (cGMP)), increasing the concentration of cGMP, which causes vasodilation, increased blood flow to penile tissue while promoting smooth muscle relaxation [4,9]. However, there were several drawbacks associated with the oral route of SC, namely its low bioavailability and slow onset of action due to the first-pass effect metabolism [10,11]. On the other hand, injection by the parenteral route may cause discomfort to the patients and requires professional skills [12]. Several studies have developed transdermal delivery systems for SC that would bypass the effects of first-pass metabolism and allows sustained drug release [13–16]. However, drug permeation was hindered by the *stratum corneum* [17].

* Corresponding author.
E-mail address: andi.dian.permana@farmasi.unhas.ac.id (A.D. Permana).

https://doi.org/10.1016/j.colsurfb.2022.113018
Received 18 September 2022; Received in revised form 9 November 2022; Accepted 10 November 2022
Available online 15 November 2022
0927-7765/© 2022 Elsevier B.V. All rights reserved.

To overcome the abovementioned issues, microneedle (MN) array technology was considered the appropriate approach. MN consists of micron-sized needles varying from 100 to 1000 μm attached to a baseplate. Due to their size, they can penetrate the *stratum corneum* to deliver drugs effectively without reaching the nerve and blood vessels and, thus, were minimally invasive (not eliciting pain or bleeding) [18,19]. Moreover, MN exhibited high drug bioavailability and was easy to self-administer. Among all types of MN, the hydrogel-forming microneedle (HFM) offers advantages as it has a higher drug-loading capacity with adjustable release rates without leaving polymeric or potentially toxic residues, unlike silicone or metallic MN [20]. The high drug-loading capacity was possible since this type of MN utilizes a drug reservoir attached to the baseplate's upper side. Upon insertion into the skin, the needle would absorb interstitial fluid and thus be swollen, allowing the drug to diffuse from the reservoir down its concentration gradient towards the hydrogel matrix and then into the skin layer, where it finally reaches the systemic circulation [21]. The capabilities of HFM to deliver a variety of molecules and drugs have been reported [22–26]. Concerning the use of HFM, it has been reported to be combined with several types of drug reservoirs, such as lyophilized and liquid reservoirs [27].

Out of all the commonly used polymers in the formulation of the HFM, poly(vinyl alcohol) (PVA) and tartaric acid were chosen for fabricating the HFM because these polymers were safe, biocompatible, and have been researched extensively [28,29]. PVA hydrogel has good water-retaining ability and was stable to temperature variation [30,31]. In addition, PVA was a water-soluble synthetic polymer that has been employed for drug-loaded HFM fabrication in combination with other polymers [32,33]. Therefore, adding poly(vinyl pyrrolidone) (PVP) in the formulation could promote a stable form for the HFM as it has the advantage of good solubility in poorly soluble drugs and was hardly affected by pH in an aqueous solution [34].

This study was the first to formulate HFM integrated with polyethylene glycol (PEG) solid dispersion as the drug reservoir containing SC for transdermal delivery. PEG could help increase the solubility and dissolution rate of drug substances, especially for drugs with low solubilities, such as SC (4.1 mg/mL in water). Therefore, it could also increase the bioavailability of SC [35,36]. This PEG solid dispersion could develop a rapidly dissolving reservoir to accommodate the limited amount of medium provided by the swollen HFM matrixes [37].

This study aims to develop and investigate different formulas for HFM to determine the potential polymers for formulating the HFM with the best SC permeation. Furthermore, a suitable formulation of the drug reservoir was also considered. The resulting system was further characterized by evaluating the insertion efficacy and drug delivery capabilities by *ex vivo* permeation studies.

2. Materials and methods

2.1. Materials

Sildenafil citrate (SC) (purity, 99.99%) of analytical grade was purchased from SMS Lifesciences India Ltd. (Telangana, India). Polyvinyl alcohol (PVA) was obtained from Sigma-Aldrich Pte Ltd. (Singapore, Singapore). Polyvinyl pyrrolidone (PVP) K-30 was purchased from Fadjar Kimia (Bogor, Indonesia). Tartaric acid, Polyethylene glycol (PEG) 1000, 4000, and 6000 were purchased from Merck Schuchardt OHG (Hohenbrunn, Germany). PEG 400 and Tween80® were purchased from idCHEM Co., Ltd. (Gyeonggi, South Korea). Tablet phosphate-buffered saline (PBS) was purchased from Dulbecco A Oxoid Ltd. (Hampshire, United Kingdom). Distilled water was purchased from PT Jayamas Medica Industri (Sidoarjo, Indonesia). All other chemicals and materials were of analytical grade.

2.2. Saturation solubility study

This study was carried out to compare the solubility of SC in various solvents and obtain a suitable release medium for *ex vivo* assays. The saturated solubility of SC was measured by placing various solvents and solvent mixtures consisting of PEG 400, Tween80®, and PBS at various pH in each vial of 1 mL. Furthermore, SC was added to the vial and homogenized with a Vortex® mixer until the solution became cloudy. Afterward, the vial was put in an orbital shaker (Optima® OS-752, Japan) at 100 rpm for 24 h at a room temperature of 37 °C. Finally, the solution was put into a small tube and centrifuged at 7000 rpm for 15 min. The supernatant was taken and filtered with a 0.20 μm syringe filter, diluted with ethanol and then measured using a UV-Vis spectrophotometer at 295.8 nm [16,38].

2.3. Preparation of hydrogel

Hydrogel films were made from PVA and PVP as polymers and tartaric acid as the crosslinking agent (Table 1). Initially, the polymer was dissolved in water until homogeneous and formed a clear, viscous solution. After that, tartaric acid was added and stirred until homogeneous. The formula was put into a centrifuge (LC-04S Centrifuge, Zenith Lab (Jiangsu) Co., LTD.) for 15 min at 3500 rpm to remove the bubbles [26]. The formula was then poured into a petri dish and dried at room temperature for 48 h. After drying, the HFM was crosslinked at 90℃, 120℃, and 150℃ for 120 min [27,39].

2.4. Swelling study

The swelling study was conducted to determine the ability of the hydrogel film to absorb the fluid. This study was essential because when the HFM was inserted into the skin, only a small amount of interstitial skin fluid (ISF) would be available. Thus, the hydrogel needed a large swelling degree to maintain the ability of HFM to swell and deliver the drug even though there was limited fluid that could be absorbed. This study was carried out by weighing the hydrogel film and then soaked in PBS pH 7.4, and then weighed again at the interval time of 0.5, 1, 2, 3, 4, 5, 10, 15, 30, 60, 120, 180, 240, 300, 360, 420, 480 min and 24 h. Before weighing, the film's surface was dried with paper to remove excess liquid. The data obtained was then calculated as the percentage of swelling to determine the maximum amount that could be absorbed by the hydrogel [27]. The swelling rate was calculated using Eq. 1, where m_1 was the weight of the 24 h swollen hydrogel and m_0 was the initial weight of the hydrogel [40].

$$\%\ \text{Swelling} = \frac{(m_1\text{-}m_0)}{m_0} \times \quad 100\% \tag{1}$$

2.5. Gel fraction analysis

The gel fraction analysis was carried out to determine the elasticity of the hydrogel, which indicates the percentage of gel fraction (%GF). The hydrogel membrane was dried in an oven at 50℃ for 24 h and then

Table 1
Hydrogel film formulation at various crosslinking temperatures.

Formula	Composition in water (%w/w)	Crosslinking Temperature (C)
F1	15% PVA, 15% PVP, 0.5% tartaric acid	90
F2	15% PVA, 15% PVP, 1% tartaric acid	
F3	15% PVA, 15% PVP, 1.5% tartaric acid	
F4	15% PVA, 15% PVP, 0.5% tartaric acid	120
F5	15% PVA, 15% PVP, 1% tartaric acid	
F6	15% PVA, 15% PVP, 1.5% tartaric acid	
F7	15% PVA, 15% PVP, 0.5% tartaric acid	150
F8	15% PVA, 15% PVP, 1% tartaric acid	
F9	15% PVA, 15% PVP, 1.5% tartaric acid	

weighed. The hydrogel membrane was soaked in distilled water for 24 h until it regained equilibrium swelling. The insoluble gel was dried in the oven at 50℃ and weighed again. The result of gel fraction (GF%) was determined by calculating the weight ratio between the insoluble dry gel weight (W_e) with the initial weight of the polymer (W_0) by Eq. 2 [41].

$$\%GF = \frac{W_e}{W_0} \times 100\% \quad (2)$$

2.6. Fabrication of hydrogel-forming microneedle (HFM)

HFM arrays were prepared using the formula in **Section 2.3** . Briefly, 0.5 g aliquot of each aqueous polymeric blend was carefully poured into the MN silicone moulds (needle density 10 ×10, conical shape, 700 μm height) and centrifuged at 3500 rpm for 15 min to remove bubbles. The HFM arrays were dried at 37℃ for 48 h. After drying, HFM arrays were removed from the moulds and heated for 2 h at 90℃, 120℃, and 150℃ to facilitate the crosslinking reaction. Upon cooling, the HFM arrays were packed and stored with silica gel for further testing [26,42].

2.7. Mechanical and insertion properties of HFM

This study has been carried out to evaluate the physical characteristics of HFM. Parafilm®M was arranged to form an eight-layer film as a validated artificial skin test model [43]. Subsequently, HFM arrays were attached to Parafilm®M. A weight of 3.2 kg, equivalent to a force of 32 N/array, equitable to the strength of manual compression, was applied on top of the HFM for 30 s [44]. After 30 s, the HFM arrays were removed, and the needle height was observed using a light microscope (Olympus® CX23, Japan). The percentage of reduction in the needle height as an interpretation of mechanical strength was determined using Eq. 3, where H_0 was needle height before compression and H_c was needle height after compression.

$$\text{Height reduction}(\%) = \frac{H0 - Hc}{H0} x100\% \quad (3)$$

Insertion properties were determined by the number of holes created in each layer of the Parafilm®M and observed using a light microscope, and the deepest layer of the hole was specified [27].

2.8. Surface pH

The surface pH evaluation was carried out to determine the surface condition of the HFM pH using a hydrogel film which was considered part of the HFM surface. This method was done by immersing 20 mg of hydrogel film in 50 mL of double distilled water and being allowed to stand at room temperature for 15 min. Next, the composite electrode was placed on the surface of the hydrogel film. The pH was measured after the equilibrium for 1 min [45].

2.9. Water vapour transmission (WVT)

This study has been carried out to determine the stability of the hydrogel against humidity by measuring the water vapour transmission ability. WVT was evaluated by sealing glass vials containing anhydrous calcium chloride using hydrogel film assisted with adhesive tape. The vials were stored in a desiccator containing saturated potassium chloride solution for 14 days [45]. WVT was calculated using Eq. 4, where V_t was the vial's final weight, and V_0 was the vial's initial weight [46].

$$WVT = \frac{(Vt\text{-}V0) \text{ x film thickness}}{\text{film surface area}} \quad (4)$$

2.10. Moisture absorption ability (MAA)

An MAA study was conducted to investigate the hydrogel film's ability to absorb moisture from different environments, indicating % MAA. Initially, hydrogel film was stored in three desiccators with different relative humidity (RH) types. Each desiccator contains magnesium chloride (33% RH), sodium nitrite (65% RH), and potassium sulfate (97% RH). Hydrogel film was stored for 14 days and weighed every 24 h. The results of this study were based on the MAA percentage calculated by Eq. 5 [47].

$$\%MAA = \frac{\text{Mass of HFM in desiccator - Initial mass of HFM}}{\text{Initial mass of HFM}} \quad (5)$$

2.11. Preparation of PEG (polyethylene glycol) reservoirs

The PEG reservoir was made using the modified solid dispersion method [27] with the compositions listed in Table 2. The PEG mixture was heated using an oven at 70℃ for 15 min to form a clear solution. The PEG mixture was removed from the oven, and the SC was added while mixing vigorously until homogeneous. The reservoir mixture was then put back into the oven for 15 min, and after that, it was poured on a silicone mould with a size of 100 mm × 100 mm and obtained a final weight of 250 mg. Lastly, the reservoir was put in the fridge (4℃) for 15 min to make the reservoir solid.

2.12. Characterization of PEG reservoirs

2.12.1. Physical properties of PEG reservoirs

The physical properties of PEG reservoirs include hardness and dissolution time. The PEG reservoir hardness test was carried out using a hardness tester (Sotax® HT1, India). The sample was placed in the instrument, and the diameter of the sample was adjusted. After that, run the test until the damage occurs and the force required to apply the pressure was shown [48]. The dissolution time of the PEG reservoir was determined visually by dissolving the reservoir in 20 mL of PBS (pH 7.4) and then stirred using a magnetic stirrer at 600 rpm at 37℃. The time required for the reservoir to fully dissolve was recorded as dissolution time [27].

2.12.2. Drug content recovery

This study was carried out to ensure the drug's stability in the form of a PEG reservoir by measuring the amount of SC presented in the reservoir. The amount of PEG reservoir equivalent to 10 mg SC was weighed and dissolved in the vial glass containing 10 mL of ethanol (96%) using a magnetic stirrer until a clear solution was obtained. The solution was then measured using spectrophotometry at the maximum wavelength of SC. The concentration obtained was then compared with the planned concentration and recorded as the drug content recovery.

2.12.3. X-ray diffraction (XRD)

The physical state of SC in the various reservoir preparations and its physical mixture was evaluated by an XRD study. The XRD patterns of all samples were determined using an X-Ray diffraction tool (Rigaku®, Japan) with a CuK α anode at 40 kV and 30 mA with a scan rate of 4°/min from 2θ range 10–90° [49].

Table 2
Composition of PEG reservoir's formula.

Composition (%w/w)	R1	R2	R3
Reservoir's Composition			
Sildenafil citrate	10	10	10
PEG mixture	90	90	90
PEG Mixture Composition			
PEG 400	–	–	40
PEG 1000	25	50	–
PEG 4000	75	50	–
PEG 6000	–	–	60

2.13. Fourier transform infrared spectroscopy (FTIR)

FTIR analysis was carried out to analyze the drug's presence and the interaction between SC and PEG in reservoir formulations and to analyze the process of crosslinking in HFM due to the change of the functional groups. The sample was analyzed using a spectrometer (Shimadzu® IR Prestige-21, Japan). The sample and 100 mg of potassium bromide (KBr) were mixed in a mortar and then pressed for 5 min at ten tones/cm^2 to form semi-transparent pellets that allow light to be transmitted to the detector for each measurement over the spectral range of 400–4000 cm^{-1} with 128 scans collected at a resolution of 4 cm^{-1} [50].

2.14. Skin preparation

The skin was obtained from a euthanized rat that had been shaved. Next, the skin was washed using a PBS solution (pH 7.4), and the fat layer was removed. Skin thickness was measured using a digital caliper (Taffware® LCD-XY, Indonesia), then wrapped in aluminum foil and stored in the freezer (temperature of −20C) for further testing.

2.15. Ex vivo permeation study

Ex vivo permeation studies were carried out using rats' skin membranes on Franz diffusion cells [45]. First, the rats' skin was soaked in PBS solution (pH 7.4) for 10 min. Then, the skin was placed in the donor compartment. The HFM was inserted into the skin, with the PEG reservoir situated on top of the HFM. A weight of 10 g each was given above the PEG reservoir to avoid any shifting during the experiment. The medium in the receptor compartment used was Tween80 2% in PBS solution (pH 7.4). This test was performed at 37 ± 1C and stirred at 100 rpm. Sampling from the receptor compartment was carried out simultaneously at intervals of 0.5, 1, 2, 3, 4, 5, 6, 7, 8, and 24 h. The results of the samples were then analyzed using spectrophotometry at the maximum wavelength of SC.

2.16. Skin integrity

FTIR was used to assess the integrity of the skin structure to determine the impact of HFM's application on the skin structure [45,51]. These studies examine the conformation of lipids and proteins in the epidermis. By comparing the displacement of infrared bands of the treated and untreated skin, it was possible to understand the changes in the stratum corneum brought on by the treatment [52]. After the *ex vivo* permeation study, the rats' skin which had been removed from the compartment, was washed and analyzed with FTIR. The comparison of treated skin with untreated skin used as a control was also investigated.

2.17. Hemolytic assay

A hemolytic assay was performed using red blood cells from rats as an initial toxicity screening for the developed preparation. First of all, blood was centrifuged at 2000 rpm for 20 min. After that, plasma was collected, and red blood cells were washed using PBS 3 times to obtain a clear supernatant. The red blood cells that had been centrifuged were then added with PBS to a final concentration of 10%v/v. The test sample was diluted using PBS and made in three concentration levels, namely 500, 50, and 5 ppm. For every 900 μL of the sample, 100 μL of red blood cell suspension was added and incubated at 37C for 60 min. In addition, positive control was also made using aquadest and a negative control using PBS. After incubation, the solution was centrifuged at 7000 rpm for 10 min, and the supernatant was sampled and measured using a UV-Vis spectrophotometer at 540 nm [16,45,53]. The hemolytic percentage of each formula was calculated using Eq. 6.

$$\%\text{Hemolytic} = \frac{\text{Sample absorbance - Negative control absorbance}}{\text{Positive control absorbance - Negative control absorbance}} \times 100\% \quad (6)$$

2.18. Statistical analysis

GraphPad Prism® version 8.0 was used for statistical analysis (GraphPad Software, San Diego, California, USA). Except when otherwise noted, all experimental results were provided as means and standard deviation (SD). The analysis of variance (ANOVA) in One-Way was performed to compare different groups. Statistical significance was always indicated by a value of $p < 0.05$.

3. Results and discussion

3.1. Saturation solubility study

SC belongs to the BCS class II group, which has poor solubility and good permeability [54]. SC requires surfactant to increase its permeability through the skin [16]. Thus, the determination of saturated solubility was carried out to determine the concentration and type of surfactant with the greatest solubility value to be used as a combination for the dissolution media. Surfactants can increase the dissolution of poorly water-soluble drugs in two ways, either by lowering the surface tension of the solid drug to increase the surface area available for dissolution or by increasing the solubility of the drug [55]. The results obtained can be seen in Table S1, which shows that the highest solubility was obtained from the combination of PBS pH 7.4 with Tween80 2% (770.2 ± 8.2 μg/mL), while the lowest solubility was obtained from PBS pH 6.8 (16.42 ± 0.31 μg/mL). Tween80 was considered a suitable co-solvent because of its high drug solubility and low risk of skin toxicity [16]. Therefore, it was used to enhance the solubility of the drug during the *ex vivo* permeation study because of its suitable surfactant properties.

3.2. Preparation of hydrogel and swelling studies

Crosslinking was a process of creating a swellable polymer structure involving hydrogel groups of polymer chains in a reaction with functional groups of crosslinkers, creating a crosslinked structure [39]. With respect to the crosslinking agent used, tartaric acid was a famous crosslinking agent with two CH_2 groups, each bearing one -OH group that could form crosslinking structure by the esterification reaction. Therefore, the swellable structure was possible by using PVA as the hydrogel polymer, which water absorption ability was due to its large number of -OH groups [39]. The addition of PVP in the formula aims to provide a structural backbone to hydrogel-forming microneedles, promoting mechanical properties [34]. In the preliminary study, we determined the fixed amount of PVA and PVP used in the formulation before subjecting it to 9 different formulas with variations in tartaric acid concentration as the crosslinking agent and varying the crosslinking temperature (Table 1).

As presented, the result showed that films prepared with 0.5% w/w tartaric acid (F1) had the highest swelling percentage when compared to the films prepared with 1% w/w and 1.5% w/w tartaric acids (F4 and F7, respectively) under a crosslinking temperature of 90 °C (Fig. 1**A**). However, as shown in Figs. 1**B** and 1**C**, the highest swelling percentage under the crosslinking temperature of 120 °C was achieved by the films prepared with 1% w/w tartaric acid (F5). In contrast, under the crosslinking temperature of 150 °C, the highest swelling percentage was achieved by the films prepared with 1.5% w/w tartaric acid (F6). Upon statistical analysis using One-Way ANOVA, it was found that there was a significant difference in each of the three conditions tested ($p < 0.05$).

The hydrogels' swelling profile affected the solute's mechanical

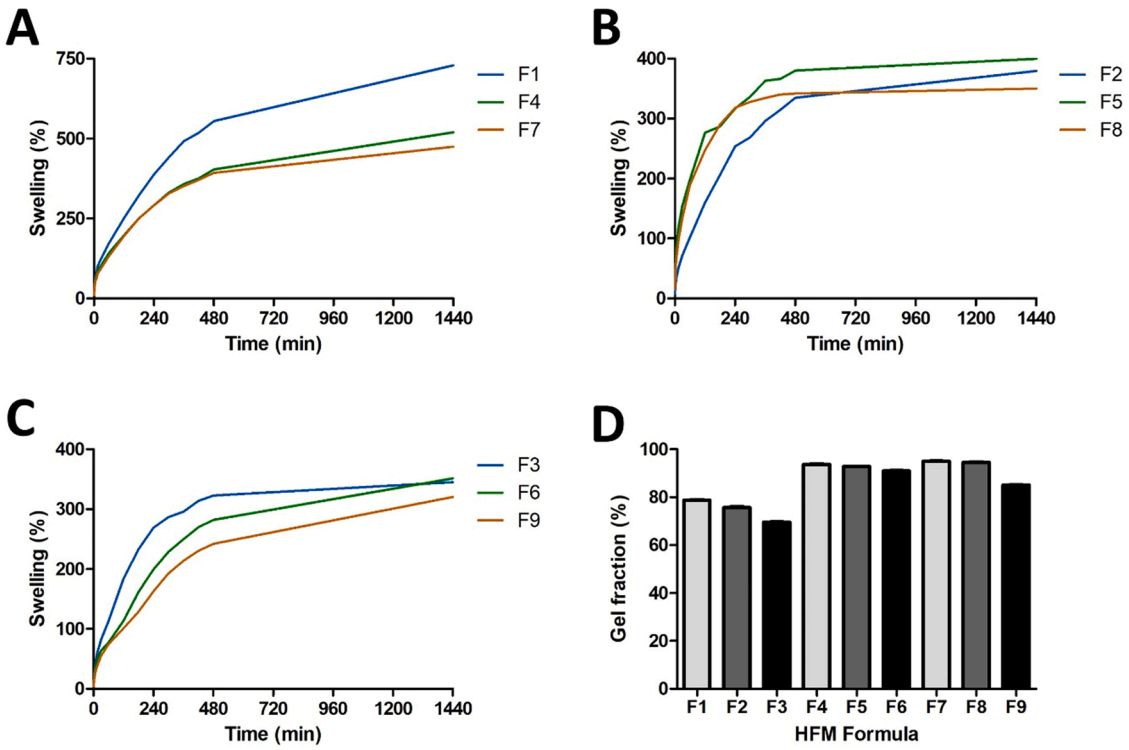

Fig. 1. Swelling behaviour of hydrogel film with different crosslink temperatures on each formula, namely 90℃ (A); 120℃ (B);150℃ (C); and percentage of gel fraction on each formula (D).

characteristics and diffusivity and was influenced by the crosslinker ratio, polymer, and crosslink temperature [20,27]. This result showed that the concentration of crosslinker and the crosslinking temperature affect the swelling ratio of the hydrogel films. This result was the same as previous study, which was expected since increasing these two parameters could increase the degree of crosslink between PVA chains and tartaric acid [56]. The higher the crosslinker agent, the lower the swelling properties may be achieved. Increasing the crosslinker concentration increases the binding of the polymers involved. Hence, the amount of water trapped inside the polymer network decreases, which causes a low swelling ratio [56]. In this case, the lower swelling degree of the highly crosslinked network was caused by the restriction of polymer chain movement.

Moreover, the swelling ratio was affected by temperature change, where increasing the temperature also increases the swelling ratio [57]. This phenomenon happens as an increase in kinetic energy for the reagents promoted by the high temperature causes an increase in water volatilization from the reaction system, which facilitates the esterification reaction. However, further increasing the temperature could form parts of the dense structure in the polymer, which deteriorates the hydrogel's swelling abilities [58].

By comparing the F1, F5, and F6 statistically, it was found that the swelling percentages between the three formulas were significantly different ($p < 0.05$), with the value of the swelling percentage, were 728,97 ± 1,30%; 399,88 ± 2,05%; and 384,07 ± 24,26%, respectively.

3.3. Gel fraction

The gel fraction study indicates the number of crosslinks between the polymers in the hydrogel, which affects the elasticity of the hydrogel [59]. The results of the gel fraction study were shown in Fig. 1**D**. It was found that decreasing the crosslinking agent concentration and increasing the temperature could increase the gel fraction according to F7, which had the lowest concentration of crosslinking agent (tartaric acid 0,5% w/w) and the highest crosslink temperature (150C). The addition of the concentration of tartaric acid (crosslinking agents) can increase the strength of the crosslinks, which causes decreased elasticity and elongation to break off the membranes [41]. Moreover, the temperature can also affect the gel fraction. As a cause of water evaporation at higher temperatures, the gel formed was smaller due to the primary chain's kinetics length shortage (which was affected by radical polymerization). Thus, the number of monomers with double bonds per chain decreases. In conclusion, the phase separation and cell formation were delayed since the probability of chain integration into the network decreased [60].

3.4. Fabrication and characterization of HFM

Previous studies have shown that the combination of PVA, which has the -OH group, and PVP, which has the C═O group, can increase the mechanical strength of microneedles due to the formation of hydrogen bonds between them [61]. In addition, as a crosslinking agent, tartaric acid bind to the -OH group through an esterification reaction and strengthen the HFM matrix [39]. The results showed that all the prepared HFM exhibited a homogeneous blend. The morphology of HFM was observed using a light microscope, and the representative image in Fig. 2**A** reveals that the HFM formed a sharp needle tip. All HFM formulations produced needles height at around 700 μm, allowing the drug to release through the epidermis into the dermis as the epidermis has a thickness of up to 180 μm. These HFM formulations would stay in the middle of the dermis and cannot go deep into the nerve to cause pain [62].

Mechanical strength was evaluated to determine the resistance of HFM to compression forces when applied to 8 layers of Parafilm®M. Needles morphologies from this assay were presented in Figs. 2**A** and 2**B**. In addition, the percentage of HFM needles height reduction from all formulations was shown in Fig. 2**D**. HFM with crosslinking degree at 90℃ has the highest percentage of needle height reduction among other HFM, which can be caused by lower crosslink temperatures resulting in the formation of HFM materials that were much softer than other HFM

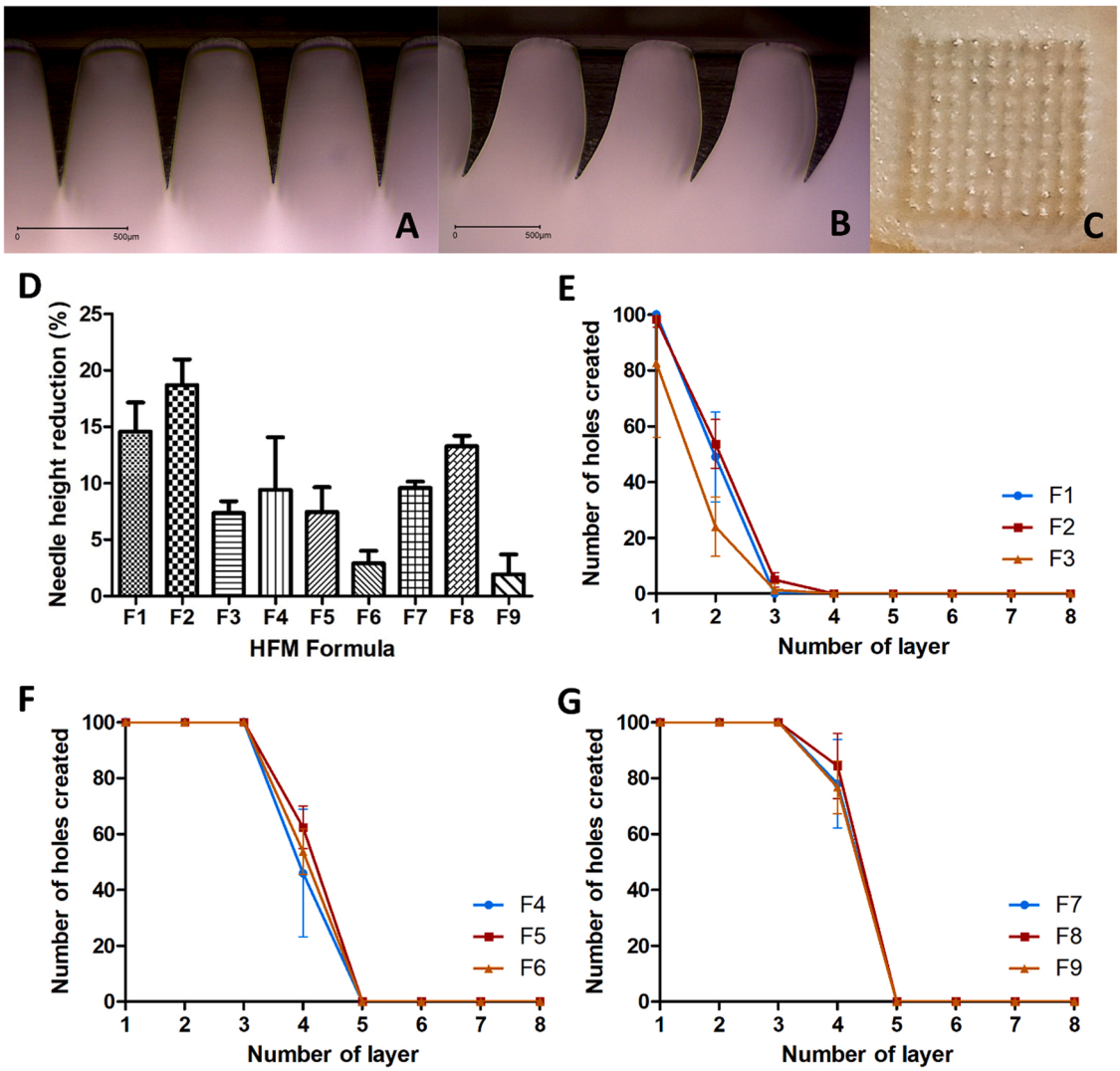

Fig. 2. Representative microscopic view of HFM (4x magnification) before (A) and after (B) penetration through Parafilm® M; representative image of rats' skin after insertion of HFM (C); comparison of mechanical strength of HFM prepared (means + SD, n = 3) (D); penetration ability of HFM on each crosslink temperature namely 90℃ (E); 120℃ (F);150℃ (G).

[27,63]. HFM with the crosslinking temperature of 120℃ and 150℃ had a percentage value of needle height reduction of < 10%. However, it was found that the crosslinking temperature of the 150℃ group, when compared to the 120℃ group, resulted in a higher percentage of needle height reduction. Statistically, the values were not significantly different ($p > 0.05$). This result indicates that these HFM formulas had adequate mechanical strength, hence, their capability to resist a compression force [64].

Insertion properties were evaluated to find out the capability of HFM to penetrate the artificial skin test model to ensure that HFM penetrates the *stratum corneum* to deliver the drug. As presented in Fig. 2**E-G**, all HFM formulas were inserted into the first two layers of Parafilm®M, but only formulas with crosslinking degrees at 120 °C and 150 °C can penetrate to the fourth layer of Parafilm®M which was equivalent to 504 μm (Parafilm®M layer thickness = 126 μm) or 72% of the total needle height. The increase in crosslinking temperature in formulas with the same concentration of tartaric acid showed an increase in the number of holes created on Parafilm®M. This exhibit that increasing the crosslinking temperature can increase the insertion properties of HFM because the HFM matrix formed becomes denser and stronger [27,63]. The best insertion property was obtained by crosslinking temperature 150℃, which penetrated the fourth layer with more holes created. Statistical analysis found no significant differences between the number of holes created in the fourth layer of groups in crosslinking temperatures of 120℃ and 150℃ ($p < 0.05$). Hence, HFM with crosslinking temperatures of 120℃ was preferable due to less heat energy required to form good HFM and skin insertion properties (Fig. 2**C**).

3.5. Surface pH

Surface pH was a parameter representing the skin's function, including the *stratum corneum*. When the pH was not suitable for the skin's surface pH (normally 4–5.5), it can cause irritation and discomfort to human skin [45,65]. The results of the surface pH evaluation were shown in Fig. 3**A**. Based on the evaluation of the F4, F5, and F7 formulas, the surface pH values are 5.32 ± 0.49, 5.11 ± 0.52, and 5.03 ± 0, 39. The surface pH values obtained by each formula were not significantly different ($p > 0.05$) and showed that the HFM formulas were non-invasive and non-irritant to the skin.

3.6. Water vapour transmission

WVT was evaluated to determine the stability of the hydrogel against humidity by measuring the water vapour transmission ability. After 14

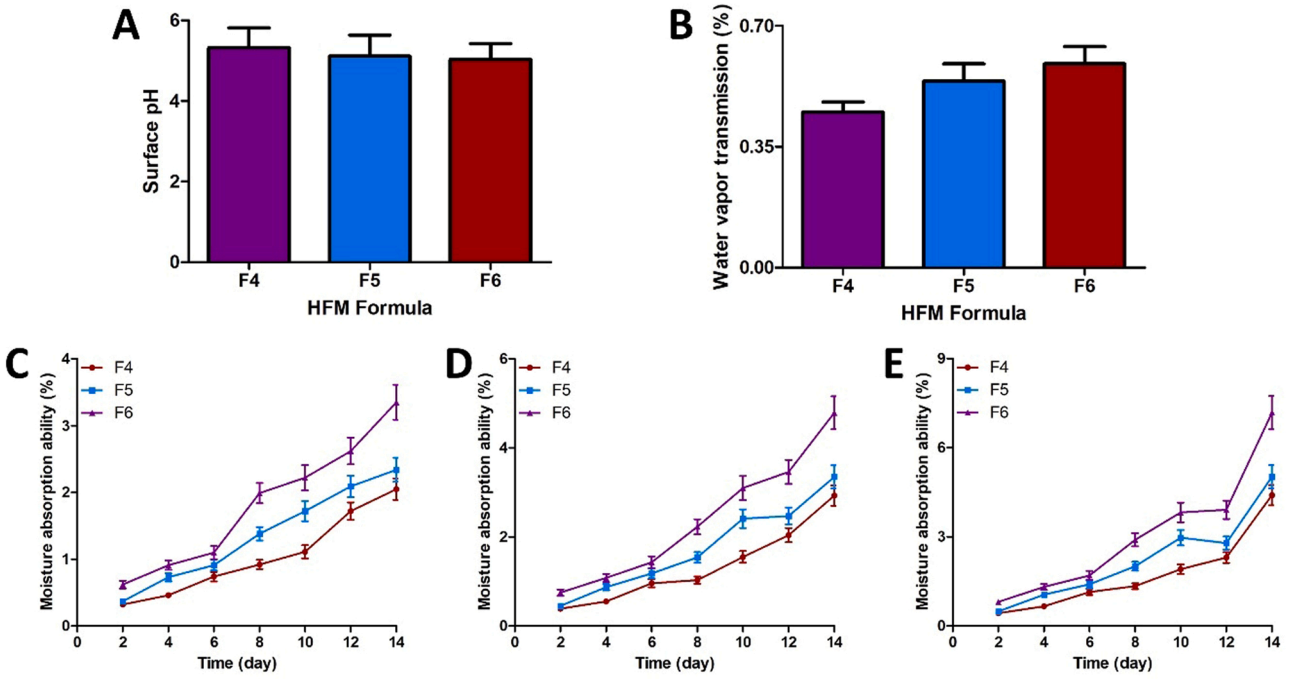

Fig. 3. Surface pH (A), water vapour transmission (B), also moisture absorption ability at RH 33% (C), RH 65% (D), and RH 97% (E) for all selected HFM formulas.

days, transmission rates were 0.45 ± 0.03, 0.54 ± 0.05, 0.59 ± 0.05 μg. cm/cm^2 for F4, F5, and F6, respectively. Statistically, the increase in WVT was not significantly different ($p > 0.05$). These results indicate lower WVT values than a previous study [66]. Hydrogel film with low WVT values, i.e., low water vapour loss capability, could indicate the long-term stability of HFM [45].

3.7. Moisture absorption ability

One of the important evaluations of HFM was the ability to absorb moisture from the environment, which affects the mechanical strength of HFM [45]. Based on Fig. 3**C-E**, the increased RH value was followed by an increase in the water absorption ability of HFM for 14 days, which had a value of < 10%. The formula with the highest concentration of tartaric acid was found to have the highest water absorption ability. This was due to the tartaric acid compound having the -COOH functional group, which increases the hygroscopicity of HFM. This was also followed by increased ability to absorb water in the air [67]. Therefore, the addition of tartaric acid concentration can affect the moisture absorption ability of HFM.

3.8. Preparation and physical properties of PEG reservoirs

Based on the preliminary study (Fig. S1 **and** Table S2), we compared several types of PEG with different molecular weights, namely PEG 400, 1000, 4000, and 6000. The three best formulas (Fig. 4**A-C**) show more optimal hardness and dissolution time than other PEG mixtures (Table 2). Hardness testing was necessary for the drug reservoir properties as the drug reservoir has to accommodate the minimum liquid medium provided by the hydrogel-forming microneedle [37]. Reservoir's hardness was the main factor that needed to be considered for physical resistance during manufacturing and transportation. Therefore, the reservoir must not be too hard or too soft. As shown in Fig. 4**H**, the hardness of the reservoir found was 29,33 N/cm^2, 24,67 N/cm^2, and 19 N/cm^2 for R1, R2, and R3, respectively. The results showed that an increase in the concentration of PEG 1000 proportions caused a decrease in the mechanical strength of the reservoir. The reservoir containing 25% PEG 1000 in R1 was significantly stronger ($p < 0.05$) than all other reservoirs containing higher PEG concentrations. The R3 has the lowest hardness because it contains PEG 400, which has the lowest molecular weight compared to other types of PEG, affecting the hardness. The hardness of the PEG reservoir was influenced by the molecular weight of the PEG used. The greater the molecular weight, the harder the resulting reservoir [27]. According to previous studies, a hardness of around 30 N was a criterion for directly compressed tablets [68,69]. Therefore, the value was used as one criterion to achieve optimum reservoir formulation.

The dissolution time was carried out to determine the PEG reservoir with the most optimal dissolution time. A comparison of the dissolution times of R1, R2, and R3 was shown in Fig. 4**G**. The results revealed that different combinations of PEG 1000 and PEG 4000 were used to generate reservoirs to accommodate SC drugs. With regard to the dissolution time, it was observed that an increase in the concentration of PEG 1000 was followed by a significant decrease ($p < 0.05$) in the dissolution rate. The increase in the dissolution rate of SC was due to the reservoir containing solid dispersion of PEG or a hydrophilic polymer that plays a vital role in increasing the dissolution and bioavailability of poorly soluble drugs [70]. The molecular weight of the polymer can affect drug dissolution, and PEG 1000 has a lower molecular weight than PEG 4000. Increasing the polymer's molecular weight can decrease the drug's solubility [71]. These results indicate that the reservoir dissolution time highly depends on the proportion of PEG 1000 and PEG 4000.

3.9. Drug content recovery

The drug recovery study was carried out to determine the amount of drug content contained in the reservoir. The results of the study show that all reservoir formulas contain more than 98% SC, which can be seen in Fig. 4**I**. These results met the requirements because the chemical requirements of the SC preparation were determined based on the drug content of not less than 98% and not more than 102% of the labeled amount of sildenafil [72]. Previous reference results explained that SC was stable and hydrolyzed under acid and alkaline conditions with a recovery percentage of more than 90% [73].

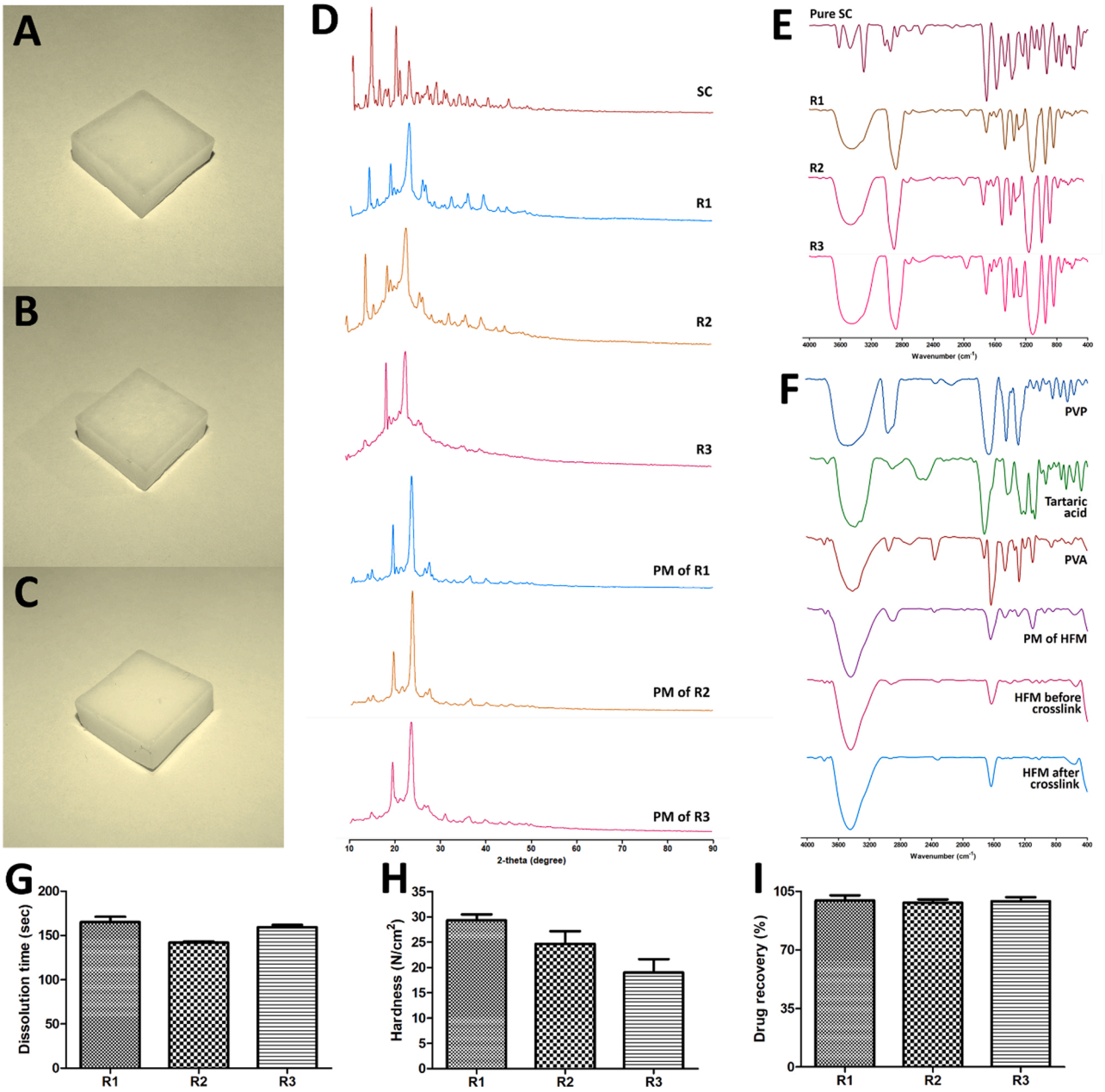

Fig. 4. The physical appearance of PEG reservoirs R1 (A), R2 (B), and R3 (C), respectively; the X-ray Diffractograms (D) and FTIR spectra (E) of pure SC, PEG reservoirs and its physical mixture; FTIR spectra of HFM and its composition (F); dissolution time (G); hardness (H); and drug content recovery of PEG reservoir (mean ± SD, n = 3).

3.10. X-ray diffraction (XRD) and fourier transform infrared spectroscopy (FTIR)

The XRD analysis on the PEG reservoir was carried out to determine the crystalline properties formed after the SC turned into a solid dispersion. The SC's crystal properties determine the SC's solubility through the form of the PEG reservoir [49,74]. In the results of the diffractogram, which can be seen in Fig. 4**D**, pure SC had a lot of sharp peaks, indicating that many developed crystalline forms were found in the material. At the same time, the PEG reservoir shape and its physical mixture showed peak intensity, indicating that SC in the formula started to reach an amorphous form that was easier to dissolve and better delivered due to increased solubility.

FTIR spectroscopy was utilized for further characterization to assess whether any interactions occurred between the drug and the reservoir. The IR spectra of pure SC and reservoirs which contains SC were shown in Fig. 4**E**. The characteristic of the SC's IR spectra was the presence of -COOH groups at 1701 cm^{-1} as a result of the citrate-ion presence [75]. Hydrogen bonds were numerous in SC complexes, usually shown as enlargement in the 2700–3600 cm^{-1} region where C-H and N-H stretching vibrations were detected [76]. As for polyethylene glycol (PEG) has a broad peak at around 3400–3500 cm^{-1}, indicating the abundance of -OH groups in the PEG structure [77]. As seen in the figure, all the observed reservoirs had peaks at 1701 cm^{-1}, which confirmed the presence of SC in the PEG reservoirs. The results, which were the sum of each component spectra, show no interactions between the drug and the reservoir studied. Therefore, rather than H-bonds forming between functional groups of the components under study, it may be believed that the drug amorphization detected by the XRD analysis was caused by SC's homogenous dispersion within the polymer

matrix blends. From the diminishing or removal of peak intensity observed in reservoir XRD data, it can be concluded that either the drug crystallinity had decreased or it had changed from crystalline to amorphous. The order of reduction of the peak intensity observed was R3-R2-R1. This might be due to the difference in the molecular weight of the PEGs combination used in the reservoir. The increase in molecular weight of PEG can promote the solubility of the drug [78]. These results also correlated with the hardness and dissolution time discussed in the previous section.

FTIR Analysis was also utilized to examine the HFM binding after crosslinking. Fig. 4**F** showed the IR spectra of the HFM polymers (PVP, tartaric acid, and PVA) as well as the physical mixture of the HFM. The PVP spectra showed the presence of very broad bands at 3000–3600 cm^{-1}, indicating the hygroscopic nature of PVP by the abundant presence of -OH groups in its structure. The more -OH groups present in a material could indicate an increased hygroscopicity of that material [79]. Another characteristic was found as it shows the strong and broad bands at 2800–3200 cm^{-1}, indicating the N-H stretching in the structure and the strong peaks at 1658 cm^{-1}, which attributes to the carbonyl group [80]. The same -OH and carbonyl peaks were also observed in the IR spectra of tartaric acid and PVA. In contrast to the polymers, the physical mixture of the HFM's IR spectra showed reduced peaks of the carbonyl and sharper peaks for the -OH bands, showing that the polymers have been mixed.

By contrasting the IR spectra of HFM before and after crosslink, we could deduce that the peaks have still been preserved. Those peaks indicated that before and after crosslink, the same functional groups remain, and the HFM might have a similar structure. However, an increase in certain peaks/areas showed that crosslinking has occurred between the polymers present in the HFM. Crosslinking of PVA chains with tartaric acid resulted in the reduction of hydroxyl groups (-OH) in PVA and an increase in the carbonyl groups (-C═O) due to the esterification process (ester formation) [81]. Compared to the spectra of HFM before crosslink, the increased intensity of -C═O peaks at around 1633 cm^{-1} indicates that crosslinking has occurred [39,82]. However, an increase was observed in the peak intensity at around 3200 – 3500 cm^{-1}. It could be explained as either a result of the -OH groups from the tartaric acid molecules, which could contribute to form a bond with one-end -OH groups, increasing the amount of free-tailed -OH molecules, or the presence of residual water content, which prevents to extract further conclusions from these graphs [81].

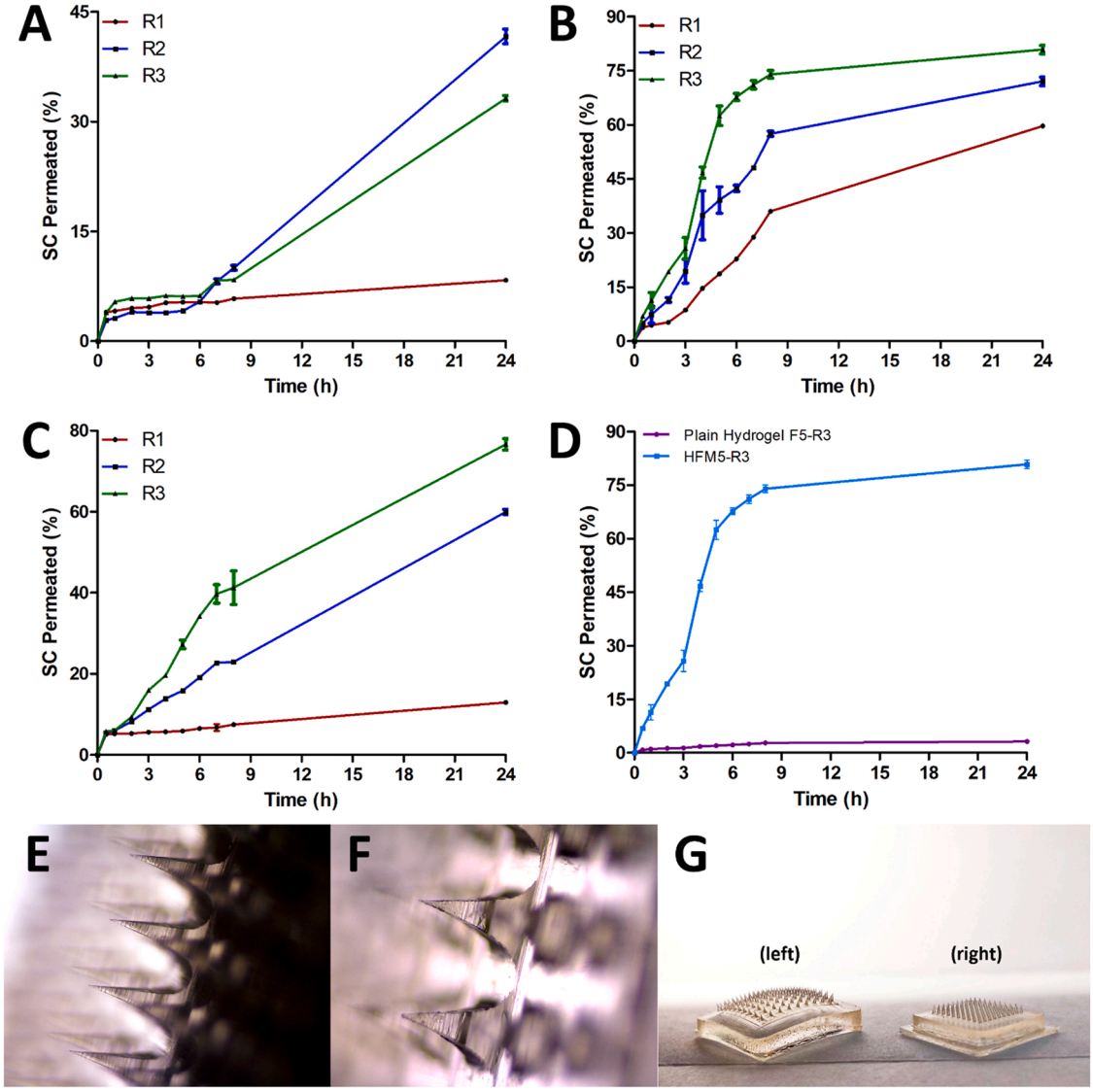

Fig. 5. *Ex vivo* permeation results on each crosslink temperature, namely 90℃ (A); 120℃ (B); 150℃ (C) with each reservoir; comparison of the permeation study of HFM5-R3 dan plain hydrogel F5-R3; the microscopic appearance of HFM before *ex vivo* test (4x magnification) (D); the microscopic appearance of HFM after *ex vivo* test (4x magnification) (E); macroscopic comparison of HFM before *ex vivo* (F right) and after *ex vivo* (F left).

3.11. Ex vivo permeation study

An *ex vivo* permeation study was carried out to determine the ability of the combination of PEG and HFM reservoirs to penetrate the *stratum corneum* and facilitate SC delivery to the systemic circulation. It should be noted that in this approach, the drug was not contained in the HFM. The drug contained in the PEG reservoir was attached on the top of HFM following the insertion of HFM in the skin. When inserted into the skin, HFM absorbs interstitial skin fluid, thereby expanding and allowing SC from the reservoir to permeate through passive diffusion. This allows the combination of the HFM and the PEG reservoir to form an unblocked channel so that the drug can continue to permeate and allow transdermal delivery with extended-release [20,37,83]. The prepared skin used in this study has a thickness of 1.32 ± 0.01 mm. The permeation profiles of the combination of HFM F4, F5, and F6 with reservoirs R1, R2, and R3 were shown in Fig. 5**A-C**. After 24 h, the SC permeated from reservoirs R1, R2, and R3 in combination with HFM F4 was 2.07 ± 0.03 mg; 10.4 ± 0.25 mg; and 8.29 ± 0.08 mg, respectively. The SC permeated from reservoirs R1, R2, and R3 in combination with HFM F5 was 14.91 ± 0.09 mg; 18 ± 0.29 mg; and 20.2 ± 0.29 mg, respectively. The SC permeated from reservoirs R1, R2, and R3 in combination with HFM F6 was 3.23 ± 0.02 mg; 14.99 ± 0.15 mg; 19.15 ± 0.35 mg, respectively.

After statistical analysis, it was found that there was a significant difference ($p < 0.05$) between the combinations of the three types of HFM and the three types of PEG reservoirs, except for the combination of F5-R1 and F6-R2. In addition, statistical analysis was carried out on the flux value (Table S3) of the HFM formula and PEG reservoir combination. Flux describes the amount of drug that can pass through an area at a particular time [84]. Hence, it was essential to determine the size and the time needed to obtain the desired pharmacological effect when the HFM was applied. The results showed that the combination had a significant difference ($p < 0.05$) between the flux values in the combination of HFM F4, F5, and F6 with the PEG R3 reservoir. These two results become a solid basis for the combination of F5-R3, which was stated to have a better permeation profile when compared to the combination of HFM and other PEG reservoirs. It also indicates that the drug released from this dosage form was about 80%, so it has the potential to provide higher bioavailability compared to other conventional dosage forms. This high permeation profile was due to the PEG composition of reservoir R3, namely PEG 400 and PEG 6000, which according to several studies, have been shown to significantly increase SC solubility [74,85].

Furthermore, Fig. 5**D** shows the permeation profile comparison between HFM F5-R3 with plain hydrogel F5-R3 to determine the effect of the microneedles system on SC release. The results showed the amount of permeated SC was 0.79 ± 0.06 mg/mL or about 3% of the drug released from this system. Statistical analysis also showed a significant difference ($p < 0.05$) between the permeation result from HFM and plain hydrogel. Therefore, the use of microneedles provides a better SC permeation profile due to a system that could open the pathway and penetrate the stratum corneum as the main skin barrier [20].

Moreover, the permeation profile of the combination of F5-R3 shows biphasic release behaviour that was marked by Hixon-Crowell release kinetics from the first 8 h with a correlation coefficient (R^2) of 0.9653, which indicates that the dissolution of the drug was significantly affected by the changes of the surface area [86,87]. Thus, the surface area for the HFM and the PEG reservoir should be considered in combining these preparations.

3.12. Skin integrity

After integrity assessment by FTIR (Fig. 6**A**), the untreated skin exhibited notable peaks at 2907 cm^{-1} due to the asymmetric stretching of the hydrocarbons, and 2751 cm^{-1}, caused by symmetric CH_2 stretching. The presence of a hydrocarbon region indicated the ceramide and fatty acid in the *stratum corneum*. Other peaks were also observed at 1683 cm-1 and 1509 cm-1, indicating the presence of amide-I and amide-II bonds in the corneocytes' keratin [51]. These peaks were also present in all treated skins with little intensity changes. The treated skin's FTIR spectra demonstrate a reduction in the height of the hydrocarbon band, indicating that the lipid was extracted from the stratum corneum. This result was in accordance with the previous study stating that PEG's capacity to enter the stratum corneum's intercellular spaces, promote fluidity, and ultimately solubilize and remove lipid components may be the primary reason for their enhancing impact [88].

Moreover, a little shift in the bands observed for amide I and amide II may be due to protein conformation change. With respect to changes in protein structure, amide bands, particularly amide-I, were sensitive to frequency shifts to higher or lower frequencies [89]. The data obtained from the FTIR analysis suggest that the HFM application did not

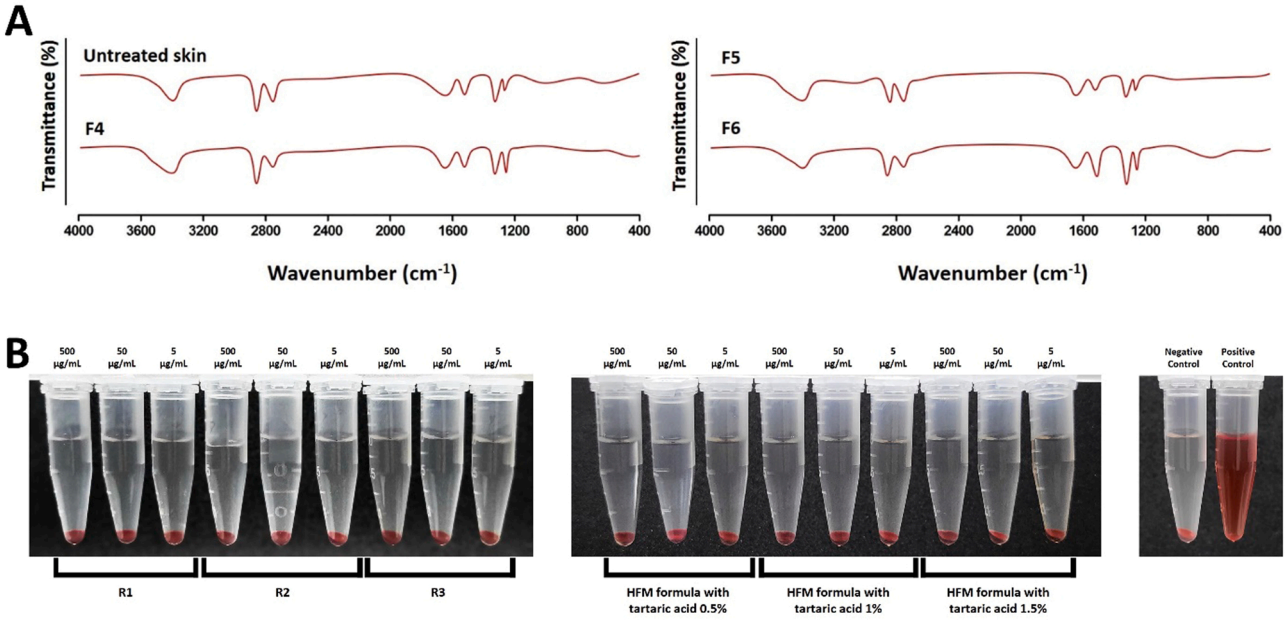

Fig. 6. FTIR result of skin integrity study (A) and the hemolytic assay of all the HFM and PEG reservoirs prepared (B).

compromise the structure of the stratum corneum. As indicated by the absence of new peaks or functional groups, there was no interaction between the elements. The minor spectral disturbance may be due to intercellular penetration caused by the PEG. However, due to the skin's suppleness and regeneration capacity, it may recover from these little changes. Overall, it could be concluded that the use of HFM was totally safe and did not cause irritation or interference with the skin barrier function. This has also been supported by several previous studies that state that repeated application of HFM has been shown to not cause skin reactions or disruptions [90,91].

3.13. Hemolytic assay

Every newly developed pharmaceutical preparation must be tested for toxicity. The hemolytic assay was one of the earliest ways to assess toxicity [45]. The results of the hemolytic assay (Fig. 6**B**) showed that no hemolytic was observed (0% of all formulas after calculation), indicating that the developed formula was not toxic to hemoglobin, as described in the previous research [92].

Finally, a combination of HFM and PEG reservoir was developed for the first time as a promising alternative therapy for ED patients. The overall results showed that this dosage form could deliver SC more quickly and has a higher potential for bioavailability via the transdermal route. This combination of preparations has also been shown to be non-irritating, non-toxic, and painless. However, the development of this dosage form was still in the early stages of drug development. Thus, further in vivo research was needed to ascertain the plasma drug concentration and determine the desired dosage.

4. Conclusion

The HFM integrated with the PEG reservoir has been successfully developed with PVA and PVP as polymers and tartaric acid as cross-linking agents. HFM has been evaluated through the swelling, mechanical, and insertion properties which showed that the matrix used can produce strong HFM and swell rapidly in the presence of interstitial fluid in the skin. The developed PEG reservoir has also been evaluated through hardness, dissolution time, as well as XRD and FTIR profiles, which showed that the reservoir has sufficient resistance for storage, and the use of PEG 400 and PEG 6000 was the best choice to facilitate its solubility. The permeation test results through rats' skin also showed that the combination of these two dosage forms was safe, painless, and non-irritating. It also has a promising advantage in increasing SC bioavailability in the treatment of erectile dysfunction.

CRediT authorship contribution statement

Diany Elim: Conceptualization, Methodology, Funding acquisition, Writing – original draft. **Andi Maqhfirah Nurul Fitri:** Methodology, Writing – original draft. **Muhammad Alif Sya'ban Mahfud:** Methodology, Writing – original draft. **Nur Afika:** Methodology, Data curation. **Nurul Aisha Fitri Sultan:** Methodology, Writing – original draft. **Hijrah:** Methodology, Data curation. **Rangga Meidianto Asri:** Data curation, Validation, Supervision **Andi Dian Permana:** Conceptualization, Project administration, Funding acquisition, Validation, Supervision, Writing – original draft.

Declaration of Competing Interest

The authors declare that they have no known competing financial interests or personal relationships that could have appeared to influence the work reported in this paper.

Data availability

No data was used for the research described in the article.

Acknowledgements

This study was fully funded by Lembaga Penelitian dan Pengabdian kepada Masyarakat (LPPM), Hasanuddin University, Indonesia, through Penelitian Dosen Penasehat Akademik (PDPA) program.

Appendix A. Supporting information

Supplementary data associated with this article can be found in the online version at doi:10.1016/j.colsurfb.2022.113018.

References

[1] A. Salonia, C. Bettocchi, L. Boeri, P. Capogrosso, J. Carvalho, N.C. Cilesiz, A. Cocci, G. Corona, K. Dimitropoulos, M. Gül, G. Hatzichristodoulou, T.H. Jones, A. Kadioglu, J.I. Martínez Salamanca, U. Milenkovic, V. Modgil, G.I. Russo, E. C. Serefoglu, T. Tharakan, P. Verze, S. Minhas, European association of urology guidelines on sexual and reproductive health—2021 update: male sexual dysfunction, Eur. Urol. 80 (2021) 333–357, https://doi.org/10.1016/j.eururo.2021.06.007.

[2] J. Saramies, M. Koiranen, J. Auvinen, H. Uusitalo, E. Hussi, S. Becker, S. Keinänen-Kiukaanniemi, J. Tuomilehto, K. Suija, Clinical medicine a natural history of erectile dysfunction in elderly men: a population-based, twelve-year prospective study, J. Clin. Med 11 (2022), https://doi.org/10.3390/jcm11082146.

[3] A. Kessler, S. Sollie, B. Challacombe, K. Briggs, M. van Hemelrijck, The global prevalence of erectile dysfunction: a review, BJU Int 124 (2019) 587–599, https://doi.org/10.1111/bju.14813.

[4] F.A. Yafi, L. Jenkins, M. Albersen, G. Corona, A.M. Isidori, S. Goldfarb, M. Maggi, C.J. Nelson, S. Parish, A. Salonia, R. Tan, J.P. Mulhall, W.J.G. Hellstrom, Erectile dysfunction, Nat. Rev. Dis. Prim. 2 (2016) 16003, https://doi.org/10.1038/nrdp.2016.3.

[5] K. Park, E.C. Hwang, S.O. Kim, Prevalence and medical management of erectile dysfunction in Asia, Asian J. Androl. 13 (2011) 543–549, https://doi.org/10.1038/aja.2010.131.

[6] D.F. Mobley, M. Khera, N. Baum, Recent advances in the treatment of erectile dysfunction, Post. Med J. 93 (2017) 679–685, https://doi.org/10.1136/postgradmedj-2016-134073.

[7] A. Manolis, M. Doumas, C. Ferri, G. Mancia, Erectile dysfunction and adherence to antihypertensive therapy: Focus on β-blockers, Eur. J. Intern Med 81 (2020) 1–6, https://doi.org/10.1016/j.ejim.2020.07.009.

[8] K.E. Andersson, PDE5 inhibitors – pharmacology and clinical applications 20 years after sildenafil discovery, Br. J. Pharm. 175 (2018) 2554–2565, https://doi.org/10.1111/bph.14205.

[9] Y. Lv, B. Yu Luo, R.R. LaBadie, H. Zhu, Y. Feng, C. Ernst, P.H. Crownover, Y. Liang, Q. Zhao, Bioequivalence and Bioavailability of an Orodispersible Tablet of Sildenafil Citrate in Healthy Chinese Male Subjects, Clin. Pharm. Drug Dev. 9 (2020) 573–581, https://doi.org/10.1002/cpdd.806.

[10] J.H. Jung, S.G. Jin, Microneedle for transdermal drug delivery: current trends and fabrication, J. Pharm. Invest. 51 (2021) 503–517, https://doi.org/10.1007/s40005-021-00512-4.

[11] A.S. Alali, M.F. Aldawsari, A. Alalaiwe, B.K. Almutairy, R. Al-Shdefat, I.A. Walbi, M.H. Fayed, Exploitation of design-of-experiment approach for design and optimization of fast-disintegrating tablets for sublingual delivery of sildenafil citrate with enhanced bioavailability using fluid-bed granulation technique, Pharmaceutics 13 (2021), https://doi.org/10.3390/pharmaceutics13060870.

[12] K. Cheung, D.B. Das, Microneedles for drug delivery: trends and progress, Drug Deliv. 23 (2016) 2338–2354, https://doi.org/10.3109/10717544.2014.986309.

[13] S.M. Badr-Eldin, O.A.A. Ahmed, Optimized nano-transfersomal films for enhanced sildenafil citrate transdermal delivery: Ex vivo and in vivo evaluation, Drug Des. Devel Ther. 10 (2016) 1323–1333.

[14] L.R. Abdelalim, O.Y. Abdallah, Y.S.R. Elnaggar, High efficacy, rapid onset nanobiolosomes of sildenafil as a topical therapy for erectile dysfunction in aged rats, Int J. Pharm. 591 (2020), 119978, https://doi.org/10.1016/j.ijpharm.2020.119978.

[15] M.K. el Sayyad, Fabrication and characterization of sildenafil citrate loaded transfersomes as a carrier for transdermal drug delivery, Pharm. Pharm. Int J. 5 (2017), https://doi.org/10.15406/ppij.2017.05.00113.

[16] A. Atipairin, C. Chunhachaichana, T. Nakpheng, N. Changsan, T. Srichana, S. Sawatdee, Development of a sildenafil citrate microemulsion-loaded hydrogel as a potential system for drug delivery to the penis and its cellular metabolic mechanism, Pharmaceutics 12 (2020) 1–23, https://doi.org/10.3390/pharmaceutics12111055.

[17] S. Dharadhar, A. Majumdar, S. Dhoble, V. Patravale, Microneedles for transdermal drug delivery: a systematic review, Drug Dev. Ind. Pharm. 45 (2019) 188–201, https://doi.org/10.1080/03639045.2018.1539497.

[18] Y. Hao, W. Li, X.L. Zhou, F. Yang, Z.Y. Qian, Microneedles-based transdermal drug delivery systems: a review, J. Biomed. Nanotechnol. 13 (2017) 1581–1597, https://doi.org/10.1166/jbn.2017.2474.

[19] Y. Ye, J. Yu, D. Wen, A.R. Kahkoska, Z. Gu, Polymeric microneedles for transdermal protein delivery, Adv. Drug Deliv. Rev. 127 (2018) 106–118, https://doi.org/10.1016/j.addr.2018.01.015.

[20] J.G. Turner, J.G. Turner, L.R. White, P. Estrela, H.S. Leese, Hydrogel-forming microneedles: current advancements and future trends, Macromol. Biosci. 2000307 (2020) 1–18, https://doi.org/10.1002/mabi.202000307.

[21] E. McAlister, B. Dutton, L.K. Vora, L. Zhao, A. Ripolin, D.S.Z.B.P.H. Zahari, H. L. Quinn, I.A. Tekko, A.J. Courtenay, S.A. Kelly, A.M. Rodgers, L. Steiner, G. Levin, E. Levy-Nissenbaum, N. Shterman, H.O. McCarthy, R.F. Donnelly, Directly compressed tablets: a novel drug-containing reservoir combined with hydrogel-forming microneedle arrays for transdermal drug delivery, Adv Healthc, Mater 10 (2021), https://doi.org/10.1002/adhm.202001256.

[22] A.J. Courtenay, E. McAlister, M.T.C. McCrudden, L. Vora, L. Steiner, G. Levin, E. Levy-Nissenbaum, N. Shterman, M.C. Kearney, H.O. McCarthy, R.F. Donnelly, Hydrogel-forming microneedle arrays as a therapeutic option for transdermal esketamine delivery, J. Control. Release 322 (2020) 177–186, https://doi.org/10.1016/j.jconrel.2020.03.026.

[23] K. Peng, L.K. Vora, J. Domínguez-Robles, Y.A. Naser, M. Li, E. Larrañeta, R. F. Donnelly, Hydrogel-forming microneedles for rapid and efficient skin deposition of controlled release tip-implants, Mater. Sci. Eng. C. 127 (2021), https://doi.org/10.1016/j.msec.2021.112226.

[24] E.M. Migdadi, A.J. Courtenay, I.A. Tekko, M.T.C. McCrudden, M.C. Kearney, E. McAlister, H.O. McCarthy, R.F. Donnelly, Hydrogel-forming microneedles enhance transdermal delivery of metformin hydrochloride, J. Control. Release 285 (2018) 142–151, https://doi.org/10.1016/j.jconrel.2018.07.009.

[25] N.N. Aung, T. Ngawhirunpat, T. Rojanarata, P. Patrojanasophon, B. Pamornpathomkul, P. Opanasopit, Fabrication, characterization and comparison of α-arbutin loaded dissolving and hydrogel forming microneedles, Int J. Pharm. 586 (2020), https://doi.org/10.1016/j.ijpharm.2020.119508.

[26] I.A. Tekko, G. Chen, J. Domínguez-Robles, R.R.S. Thakur, I.M.N. Hamdan, L. Vora, E. Larrañeta, J.C. McElnay, H.O. McCarthy, M. Rooney, R.F. Donnelly, Development and characterisation of novel poly (vinyl alcohol)/poly (vinyl pyrrolidone)-based hydrogel-forming microneedle arrays for enhanced and sustained transdermal delivery of methotrexate, Int J. Pharm. 586 (2020), 119580, https://doi.org/10.1016/j.ijpharm.2020.119580.

[27] Q.K. Anjani, A.D. Permana, Á. Cárcamo-Martínez, J. Domínguez-Robles, I. A. Tekko, E. Larrañeta, L.K. Vora, D. Ramadon, R.F. Donnelly, Versatility of hydrogel-forming microneedles in in vitro transdermal delivery of tuberculosis drugs, Eur. J. Pharm. Biopharm. 158 (2021) 294–312, https://doi.org/10.1016/j.ejpb.2020.12.003.

[28] S. Yang, Y. Feng, L. Zhang, N. Chen, W. Yuan, T. Jin, A scalable fabrication process of polymer microneedles, Int J. Nanomed. 7 (2012) 1415–1422, https://doi.org/10.2147/IJN.S28511.

[29] R. He, Y. Niu, Z. Li, A. Li, H. Yang, F. Xu, F. Li, A hydrogel microneedle patch for point-of-care testing based on skin interstitial fluid, adv healthc, Mater 9 (2020), https://doi.org/10.1002/adhm.201901201.

[30] J.I. Daza Agudelo, M.R. Ramirez, E.R. Henquin, I. Rintoul, Modelling of swelling of PVA hydrogels considering non-ideal mixing behaviour of PVA and water, J. Mater. Chem. B. 7 (2019) 4049–4054, https://doi.org/10.1039/c9tb00243j.

[31] M. Wang, J. Bai, K. Shao, W. Tang, X. Zhao, D. Lin, S. Huang, C. Chen, Z. Ding, J. Ye, Poly(vinyl alcohol) Hydrogels: The Old and New Functional Materials, Int J. Polym. Sci. (2021)) (2021), https://doi.org/10.1155/2021/2225426.

[32] T.S. Gaaz, A.B. Sulong, M.N. Akhtar, A.A.H. Kadhum, A.B. Mohamad, A.A. Al-Amiery, D.J. McPhee, Properties and applications of polyvinyl alcohol, halloysite nanotubes and their nanocomposites, Molecules 20 (2015) 22833–22847, https://doi.org/10.3390/molecules201219884.

[33] H.X. Nguyen, B.D. Bozorg, Y. Kim, A. Wieber, G. Birk, D. Lubda, A.K. Banga, Poly (vinyl alcohol) microneedles: fabrication, characterization, and application for transdermal drug delivery of doxorubicin, Eur. J. Pharm. Biopharm. 129 (2018) 88–103, https://doi.org/10.1016/j.ejpb.2018.05.017.

[34] S.J. Yang, J.O. Jeong, Y.M. Lim, J.S. Park, Synthesis and characterization of PVP microneedle patch using metal bioelectrodes for novel drug delivery system, Mater. Des. 201 (2021), https://doi.org/10.1016/j.matdes.2021.109485.

[35] F.H. Pirhayati, A. Shayanfar, A. Fathi-Azarbayjani, F. Martinez, S. Sajedi-Amin, A. Jouyban, Thermodynamic solubility and density of sildenafil citrate in ethanol and water mixtures: Measurement and correlation at various temperatures, J. Mol. Liq. 225 (2017) 631–635, https://doi.org/10.1016/j.molliq.2016.11.055.

[36] I.A. Tekko, O.M. Ali, T. Hatahet, M.F. Chehna, Polyethylene glycol-based solid dispersions to enhance eprosartan mesylate dissolution and bioavailability, Arch. Pharm. Pharmacol. Res. 2 (2019), https://doi.org/10.33552/appr.2019.02.000537.

[37] R.F. Donnelly, M.T.C. McCrudden, A.Z. Alkilani, E. Larrañeta, E. McAlister, A. J. Courtenay, M.C. Kearney, T.R. Raj Singh, H.O. McCarthy, V.L. Kett, E. Caffarel-Salvador, S. Al-Zahrani, A.D. Woolfson, Hydrogel-forming microneedles prepared from "super swelling" polymers combined with lyophilised wafers for transdermal drug delivery, PLoS One 9 (2014) 1–12, https://doi.org/10.1371/journal.pone.0111547.

[38] M.C. Kearney, P.E. McKenna, H.L. Quinn, A.J. Courtenay, E. Larrañeta, R. F. Donnelly, Design and development of liquid drug reservoirs for microneedle delivery of poorly soluble drug molecules, Pharmaceutics 11 (2019) 1–17, https://doi.org/10.3390/pharmaceutics11110605.

[39] A.K. Sonker, V. Verma, Influence of crosslinking methods toward poly(vinyl alcohol) properties: Microwave irradiation and conventional heating, J. Appl. Polym. Sci. (2018) 1–8, https://doi.org/10.1002/app.46125.

[40] T.R. Raj Singh, P.A. McCarron, A.D. Woolfson, R.F. Donnelly, Investigation of swelling and network parameters of poly(ethylene glycol)-crosslinked poly(methyl vinyl ether-co-maleic acid) hydrogels, Eur. Polym. J. 45 (2009) 1239–1249, https://doi.org/10.1016/j.eurpolymj.2008.12.019.

[41] E.A. Kamoun, E.R.S. Kenawy, T.M. Tamer, M.A. El-Meligy, M.S.Mohy Eldin, Poly (vinyl alcohol)-alginate physically crosslinked hydrogel membranes for wound dressing applications: Characterization and bio-evaluation, Arab. J. Chem. 8 (2015) 38–47, https://doi.org/10.1016/j.arabjc.2013.12.003.

[42] X. Pan, Y. Li, W. Pang, Y. Xue, Z. Wang, C. Jiang, C. Shen, Q. Liu, L. Liu, Preparation, characterisation and comparison of glabridin-loaded hydrogel-forming microneedles by chemical and physical cross-linking, Int J. Pharm. 617 (2022), https://doi.org/10.1016/j.ijpharm.2022.121612.

[43] E. Larrañeta, J. Moore, E.M. Vicente-Pérez, P. González-Vázquez, R. Lutton, A. D. Woolfson, R.F. Donnelly, A proposed model membrane and test method for microneedle insertion studies, Int J. Pharm. 472 (2014) 65–73, https://doi.org/10.1016/j.ijpharm.2014.05.042.

[44] A.D. Permana, M.T.C. McCrudden, R.F. Donnelly, Enhanced intradermal delivery of nanosuspensions of antifilariasis drugs using dissolving microneedles: A proof of concept study, Pharmaceutics 11 (2019) 346.

[45] P.W.R. Ananda, D. Elim, H.S. Zaman, W. Muslimin, M.G.R. Tunggeng, A. D. Permana, Combination of transdermal patches and solid microneedles for improved transdermal delivery of primaquine, Int J. Pharm. 609 (2021) 1–10, https://doi.org/10.1016/j.ijpharm.2021.121204.

[46] R.K. Basha, K. Konno, H. Kani, T. Kimura, Water vapor transmission rate of biomass based film materials, Engineering in Agriculture, Environment and Food 4 (2011) 37–42.

[47] L. Rahman, R.S. Lembang, S. Lallo, S.R. Handayani, A.D. Usmanengsi, Permana, Bioadhesive dermal patch as promising approach for improved antibacterial activity of bioactive compound of Zingiber cassumunar Roxb in ex vivo Staphylococcus aureus skin infection model, J. Drug Deliv. Sci. Technol. 63 (2021), 102522, https://doi.org/10.1016/j.jddst.2021.102522.

[48] Z. Wang, X. Ren, H. Feng, D. Luo, Research on the counter-force calibration method of tablet hardness tester, Meas.: Sens. 18 (2021), https://doi.org/10.1016/j.measen.2021.100233.

[49] M. Manzoor, S.A. Raza, M.H. Asim, N.I. Bukhari, S. Arshad, U. Zafar, Safety and pharmaceutical evaluation of a novel natural polymer, ocicum, as solubility and dissolution enhancer in solid dispersion, Pharmaceuticals 15 (2022), https://doi.org/10.3390/ph15070869.

[50] H. Seçilmiş Canbay, M. Doğantürk, Compatibility Studies of Sildenafil with Different Excipients by Using TGA, DSC, XRD and FTIR, Celal Bayar Üniversitesi Fen. Bilim. Derg. 15 (2019) 401–407, https://doi.org/10.18466/cbayarfbe.613951.

[51] S. Talib, N. Ahmed, D. Khan, G.M. Khan, A. ur Rehman, Chitosan-chondroitin based artemether loaded nanoparticles for transdermal drug delivery system, J. Drug Deliv. Sci. Technol. 61 (2021), https://doi.org/10.1016/j.jddst.2020.102281.

[52] A.L.M. Ruela, A.G. Perissinato, M.E. de, S. Lino, P.S. Mudrik, G.R. Pereira, Evaluation of skin absorption of drugs from topical and transdermal formulations, Braz. J. Pharm. Sci. 52 (2016) 527–544, https://doi.org/10.1590/s1984-82502016000300018.

[53] M. Mir, A.D. Permana, I.A. Tekko, H.O. McCarthy, N. Ahmed, A. ur Rehman, R. F. Donnelly, Microneedle liquid injection system assisted delivery of infection responsive nanoparticles: A promising approach for enhanced site-specific delivery of carvacrol against polymicrobial biofilms-infected wounds, Int J. Pharm. 587 (2020) 1–12, https://doi.org/10.1016/j.ijpharm.2020.119643.

[54] C. Miranda, Z. Pérez-Rodríguez, R. Hernández-Armengol, Y. Quiñones-García, T. Betancourt-Purón, M.Á. Cabrera-Pérez, Biowaiver or Bioequivalence: Ambiguity in Sildenafil Citrate BCS Classification, AAPS PharmSciTech 19 (2018) 1693–1698, https://doi.org/10.1208/s12249-018-0982-7.

[55] M. Li, N. Qiao, K. Wang, Influence of sodium lauryl sulfate and Tween 80 on carbamazepine-nicotinamide cocrystal solubility and dissolution behaviour, Pharmaceutics 5 (2013) 508–524, https://doi.org/10.3390/pharmaceutics5040508.

[56] H. Chavda, C. Patel, Effect of crosslinker concentration on characteristics of superporous hydrogel, Int J. Pharm. Invest. 1 (2011) 17–21, https://doi.org/10.4103/2230-973x.76724.

[57] A.K. Hussein, B.I. Khalil, H.H. Abud, Effect of Crosslinking Agent Ratio and Temperature on Degree of Swelling in Polymer Hydrogels, Chem. Process Eng. Res. 52 (2017) 1–9. ⟨https://www.researchgate.net/publication/320106668⟩.

[58] T. Tan, J. Zhou, X. Gao, X. Tang, H. Zhang, Synthesis, characterization and water-absorption behavior of tartaric acid-modified cellulose gel fromcorn stalk pith, Ind. Crops Prod. 169 (2021), https://doi.org/10.1016/j.indcrop.2021.113641.

[59] M.T.S. Alcântara, A.J.C. Brant, D.R. Giannini, J.O.C.P. Pessoa, A.B. Andrade, H. G. Riella, A.B. Lugão, Influence of dissolution processing of PVA blends on the characteristics of their hydrogels synthesized by radiation-Part I: Gel fraction, swelling, and mechanical properties, Radiat. Phys. Chem. 81 (2012) 1465–1470, https://doi.org/10.1016/j.radphyschem.2012.01.048.

[60] S. Qavi, S. Pourmahdian, H. Eslami, Acrylamide hydrogels preparation via free radical crosslinking copolymerization: Kinetic study and morphological investigation, J. Macromol. Sci., Part A: Pure Appl. Chem. 51 (2014) 842–848, https://doi.org/10.1080/10601325.2014.937132.

[61] A.D. Permana, Q.K. Anjani, Sartini, E. Utomo, F. Volpe-Zanutto, A.J. Paredes, Y. M. Evary, S.A. Mardikasari, M.R. Pratama, I.N. Tuany, R.F. Donnelly, Selective delivery of silver nanoparticles for improved treatment of biofilm skin infection using bacteria-responsive microparticles loaded into dissolving microneedles, Mater. Sci. Eng. C. 120 (2021), 111786.

[62] A.Z. Alkilani, M.T.C. Mccrudden, R.F. Donnelly, Transdermal drug delivery: innovative pharmaceutical developments based on disruption of the barrier properties of the stratum corneum, Pharmaceutics 7 (2015) 438–470, https://doi.org/10.3390/pharmaceutics7040438.

[63] E. Rynkowska, K. Fatyeyeva, S. Marais, J. Kujawa, W. Kujawski, Chemically and thermally crosslinked PVA-based membranes: Effect on swelling and transport behavior, Polym. (Basel) 11 (2019) 1–18, https://doi.org/10.3390/polym11111799.
[64] A.D. Permana, I.A. Tekko, M.T.C. McCrudden, Q.K. Anjani, D. Ramadon, H. O. McCarthy, R.F. Donnelly, Solid lipid nanoparticle-based dissolving microneedles: A promising intradermal lymph targeting drug delivery system with potential for enhanced treatment of lymphatic filariasis, J. Control. Release 316 (2019) 34–52, https://doi.org/10.1016/j.jconrel.2019.10.004.
[65] Chaitra Prakash, P. Bhargava, S. Tiwari, B. Majumdar, R. Kumar Bhargava, P. Bhargava, M. are, SKIN SURFACE pH IN ACNE VULGARIS: Insights from an Observational Study and Review of the Literature, 2017.
[66] M.L. Cacicedo, G. Pacheco, G.A. Islan, V.A. Alvarez, H.S. Barud, G.R. Castro, Chitosan-bacterial cellulose patch of ciprofloxacin for wound dressing: Preparation and characterization studies, Int J. Biol. Macromol. 147 (2020) 1136–1145, https://doi.org/10.1016/j.ijbiomac.2019.10.082.
[67] S. Han, J. Hong, Q. Luo, H. Xu, H. Tan, Q. Wang, J. Tao, Y. Zhou, L. Peng, Y. He, J. Shi, N. Ma, Y. Cheng, H. Su, Hygroscopicity of organic compounds as a function of organic functionality, water solubility, molecular weight and oxidation level, Atmos. Chem. Phys. (2022) 3985–4004, https://doi.org/10.5194/acp-2021-486.
[68] S. Chono, K. Nakamura, M. Matsui, Physical properties of lansoprazole orally disintegrating tablets, J. Generic Med (2017) 5–8.
[69] L.L. Augsburger, S.W. Hoag, Pharmaceutical dosage forms, Capsules (2017).
[70] M.F. Aldawsari, M.K. Anwer, M.M. Ahmed, F. Fatima, G.A. Soliman, S. Bhatia, A. Zafar, M.A. Aboudzadeh, Enhanced dissolution of sildenafil citrate using solid dispersion with hydrophilic polymers: Physicochemical characterization and in vivo sexual behavior studies in male rats, Polym. (Basel) 13 (2021), https://doi.org/10.3390/polym13203512.
[71] P.P. Lestari, E. Budianto, in: J. Phys Conf Ser (Ed.), Controlled Drug Delivery Carrier of Nifedipine Using Biodegradable Microcapsule Polymer from Poly (D,L-Lactic Acid) and Polyethylene Glycol, IOP Publishing Ltd, 2021, https://doi.org/10.1088/1742-6596/1751/1/012082.
[72] The United States Pharmacopeia, USP 36 - NF 31, United Book Press Inc., Baltimore, 2013.
[73] A.S. Yoon, S. Sawatdee, C. Woradechakul, K. Sae Chee, A. Atipairin, Physicochemical and microbiological stability of the extemporaneous sildenafil citrate oral suspension, Sci. Pharm. 83 (2015) 659–670, https://doi.org/10.3797/scipharm.1505-08.
[74] R.P. Patel, D.J. Patel, D.B. Bhimani, J.K. Patel, Physicochemical characterization and dissolution study of solid dispersions of furosemide with polyethylene glycol 6000 and polyvinylpyrrolidone k30, Dissolut Technol. 15 (2008) 17–25, https://doi.org/10.14227/DT150308P17.
[75] P. Melnikov, P.P. Corbi, A. Cuin, M. Cavicchioli, W.R. Guimarães, Physicochemical Properties of Sildenafil Citrate (Viagra) and Sildenafil Base, J. Pharm. Sci. 92 (2003) 2140–2143.
[76] A. Bozdoğan, B. Aksakal, C. Denktaş, Y. Salt, Prestretching effect and recovery process of polyvinyl alcohol film crosslinked with tartaric acid, J. Appl. Polym. Sci. 137 (2020), https://doi.org/10.1002/app.49421.
[77] F. Askari, M. Zandi, P. Shokrolahi, M.H. Tabatabaei, E. Hajirasoliha, Reduction in protein absorption on ophthalmic lenses by PEGDA bulk modification of silicone acrylate-based formulation, Prog. Biomater. 8 (2019) 169–183, https://doi.org/10.1007/s40204-019-00119-x.
[78] N. Bolourchian, M.M. Mahboobian, S. Dadashzadeh, The effect of PEG molecular weights on dissolution behavior of simvastatin in solid dispersions, Iran. J. Pharm. Res. 12 (2013) 11–20.
[79] S. Han, J. Hong, Q. Luo, H. Xu, H. Tan, Q. Wang, J. Tao, Y. Zhou, L. Peng, Y. He, J. Shi, N. Ma, Y. Cheng, H. Su, Hygroscopicity of organic compounds as a function of organic functionality, water solubility, molecular weight and oxidation level, Atmos. Chem. Phys.: Discuss. ((2021), https://doi.org/10.5194/acp-2021-486.
[80] G.M. el Maghraby, R.N. Elsergany, Fast disintegrating tablets of nisoldipine for intra-oral administration, Pharm. Dev. Technol. 19 (2014) 641–650, https://doi.org/10.3109/10837450.2013.813543.
[81] A. Bozdoğan, B. Aksakal, C. Denktaş, Y. Salt, Prestretching effect and recovery process of polyvinyl alcohol film crosslinked with tartaric acid, J. Appl. Polym. Sci. 137 (2020) 1–15, https://doi.org/10.1002/app.49421.
[82] K. Deshmukh, M. Basheer Ahamed, S. Sankaran, S.K. Khadheer Pasha, K. Kumar Sadasivuni, D. Ponnamma, M. Al-Ali Almaadeed, Studies on the Mechanical, Morphological and Electrical Properties of Highly Dispersible Graphene Oxide Reinforced Polypyrrole and Polyvinylalcohol Blend Composites, in: Mater Today Proc, Elsevier Ltd, 2018, pp. 8744–8752, https://doi.org/10.1016/j.matpr.2017.12.301.
[83] R.F. Donnelly, T.R.R. Singh, M.J. Garland, K. Migalska, R. Majithiya, C. M. McCrudden, P.L. Kole, T.M.T. Mahmood, H.O. McCarthy, A.D. Woolfson, Hydrogel-forming microneedle arrays for enhanced transdermal drug delivery, Adv. Funct. Mater. 22 (2012) 4879–4890, https://doi.org/10.1002/adfm.201200864.
[84] M. Silva-Abreu, L.C. Espinoza, L. Halbaut, M. Espina, M.L. García, A.C. Calpena, Comparative study of Ex Vivo transmucosal permeation of pioglitazone nanoparticles for the treatment of Alzheimer's disease, Polym. (Basel) 10 (2018), https://doi.org/10.3390/polym10030316.
[85] F.H. Pirhayati, A. Shayanfar, E. Rahimpour, M. Barzegar-Jalali, F. Martinez, A. Jouyban, Solubility of sildenafil citrate in polyethylene glycol 400 + water mixtures at various temperatures, J. Mol. Liq. 240 (2017) 268–272, https://doi.org/10.1016/j.molliq.2017.05.057.
[86] S. Dash, P.N. Murthy, L. Nath, P. Chowdhury, Kinetic modeling on drug release from controlled drug delivery systems, Acta Pol. Pharm. - Drug Res. 67 (2010) 217–223.
[87] H. Baishya, Application of Mathematical Models in Drug Release Kinetics of Carbidopa and Levodopa ER Tablets, J. Dev. Drugs 6 (2017) 1–8, https://doi.org/10.4172/2329-6631.1000171.
[88] A. Casiraghi, M. di Grigoli, F. Cilurzo, C.G.M. Gennari, G. Rossoni, P. Minghetti, The influence of the polar head and the hydrophobic chain on the skin penetration enhancement effect of poly(ethylene glycol) derivatives, AAPS PharmSciTech 13 (2012) 247–253, https://doi.org/10.1208/s12249-011-9745-4.
[89] H.K. Vaddi, P.C. Ho, S.Y. Chan, Terpenes in propylene glycol as skin-penetration enhancers: permeation and partition of haloperidol, fourier transform infrared spectroscopy, and differential scanning calorimetry, J. Pharm. Sci. 91 (2002) 1639–1651.
[90] R. Al-Kasasbeh, A.J. Brady, A.J. Courtenay, E. Larrañeta, M.T.C. McCrudden, D. O'Kane, S. Liggett, R.F. Donnelly, Evaluation of the clinical impact of repeat application of hydrogel-forming microneedle array patches, Drug Deliv. Transl. Res 10 (2020) 690–705, https://doi.org/10.1007/s13346-020-00727-2.
[91] E.M. Vicente-Perez, E. Larrañeta, M.T.C. McCrudden, A. Kissenpfennig, S. Hegarty, H.O. McCarthy, R.F. Donnelly, Repeat application of microneedles does not alter skin appearance or barrier function and causes no measurable disturbance of serum biomarkers of infection, inflammation or immunity in mice in vivo, Eur. J. Pharm. Biopharm. 117 (2017) 400–407, https://doi.org/10.1016/j.ejpb.2017.04.029.
[92] H.Y. Zhou, Y.P. Zhang, W.F. Zhang, X.G. Chen, Biocompatibility and characteristics of injectable chitosan-based thermosensitive hydrogel for drug delivery, Carbohydr. Polym. 83 (2011) 1643–1651, https://doi.org/10.1016/j.carbpol.2010.10.022.